Cytochrome P450 Compound I: Capture, Characterization, and C-H Bond Activation Kinetics

Jonathan Rittle and Michael T. Green

Science **330**, 933 (2010);
DOI: 10.1126/science.1193478

Science (print ISSN 0036-8075; online ISSN 1095-9203) is published weekly, except the last week in December, by the American Association for the Advancement of Science, 1200 New York Avenue NW, Washington, DC 20005.

Cytochrome P450 Compound I: Capture, Characterization, and C-H Bond Activation Kinetics

Jonathan Rittle and Michael T. Green*

Cytochrome P450 enzymes are responsible for the phase I metabolism of approximately 75% of known pharmaceuticals. P450s perform this and other important biological functions through the controlled activation of C-H bonds. Here, we report the spectroscopic and kinetic characterization of the long-sought principal intermediate involved in this process, P450 compound I (P450-I), which we prepared in approximately 75% yield by reacting ferric CYP119 with *m*-chloroperbenzoic acid. The Mössbauer spectrum of CYP119-I is similar to that of chloroperoxidase compound I, although its electron paramagnetic resonance spectrum reflects an increase in $|J|/D$, the ratio of the exchange coupling to the zero-field splitting. CYP119-I hydroxylates the unactivated C-H bonds of lauric acid [D(C-H) ~ 100 kilocalories per mole], with an apparent second-order rate constant of $k_{app} = 1.1 \times 10^7$ per molar per second at 4°C. Direct measurements put a lower limit of $k \geq 210$ per second on the rate constant for bound substrate oxidation, whereas analyses involving kinetic isotope effects predict a value in excess of 1400 per second.

Cytochrome P450s are thiolate-ligated heme enzymes that use dioxygen and the formal equivalents of molecular hydrogen ($2H^+$ and $2e^-$) to functionalize a wide range of biologically active compounds (*1*, *2*). Interest in these systems stems not only from their obvious medical and biological importance but also from a desire to harness their synthetic potential. P450s hydroxylate unactivated C-H bonds (*3*–*5*), which are ubiquitous and rather unreactive in organic molecules (*6*, *7*). A major goal of bioinorganic chemistry has been the elucidation of factors that determine P450s' ability to activate inert C-H bonds (*8*–*12*). Central to these efforts have been attempts to obtain electronic and structural characterizations of the highly reactive intermediate, termed compound I, that is thought to be responsible for these demanding oxidations (*5*, *12*–*19*).

P450 compound I (P450-I) is postulated to be an iron(IV)oxo (or ferryl) species with an additional oxidizing equivalent delocalized over the porphyrin and thiolate ligands. This species has for the most part eluded spectroscopic detection. It is not seen under normal turnover conditions but has been generated transiently in stopped-flow reactions (via the peroxide shunt pathway) (*2*). In each case, this reactive intermediate was prepared in low yield, and the reported ultraviolet (UV)/visible spectrum was extracted from the data set by using mathematical techniques (global analysis) (*2*, *20*–*22*).

Insights into the electronic and geometric structures of P450-I have come from theoretical calculations and comparisons with the enzyme chloroperoxidase (CPO). This thiolate-ligated heme-protein has served as an important (but limited) model system for the study of P450 chemistry. CPO compound I (CPO-I) is stable enough to be prepared in high yield, and detailed electronic and structural characterizations of CPO-I have been reported (*23*–*28*). However, it is clear that substantial differences exist between this species and the more reactive P450-I. CPO-I does not oxidize unactivated hydrocarbons, and it only sluggishly hydroxylates benzylic hydrogens [D(C-H) ~ 89 kcal/mol] (*29*). Evidence suggests that this difference in reactivity cannot be explained in terms of substrate access alone (*30*, *31*). The aliphatic termini of fatty acids [D(C-H) ~ 100 kcal/mol] readily access the active site of CPO-I, yet no reaction is observed.

P450-I does not accumulate during turnover, and no kinetic studies have yet fully confirmed generation of the species and subsequently tracked its reaction with substrate (*21*, *32*–*34*). The inability of researchers to "see compound I in action" has led some to question its competence as a hydroxylating species and its role in

Department of Chemistry, Pennsylvania State University, University Park, PA 16802, USA.

*To whom correspondence should be addressed. E-mail: mtg10@psu.edu

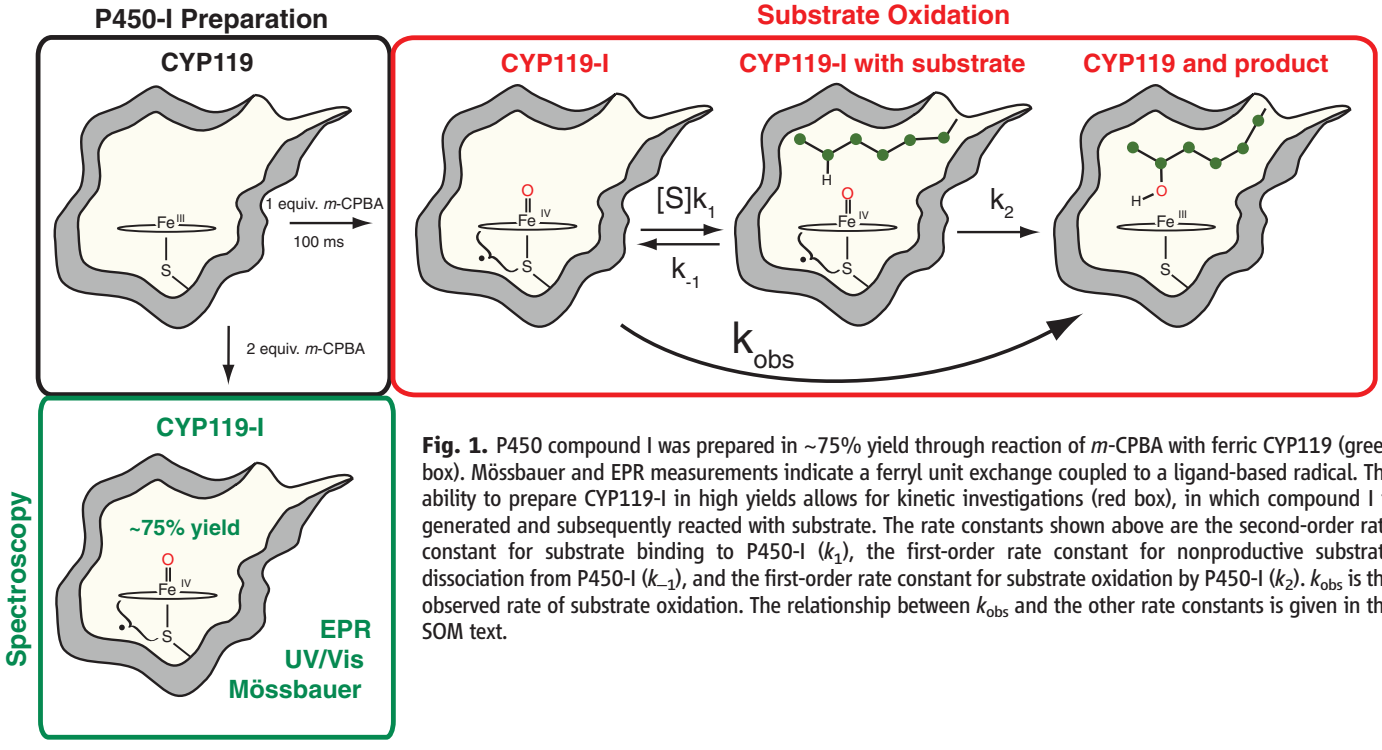

Fig. 1. P450 compound I was prepared in ~75% yield through reaction of *m*-CPBA with ferric CYP119 (green box). Mössbauer and EPR measurements indicate a ferryl unit exchange coupled to a ligand-based radical. The ability to prepare CYP119-I in high yields allows for kinetic investigations (red box), in which compound I is generated and subsequently reacted with substrate. The rate constants shown above are the second-order rate constant for substrate binding to P450-I (k_1), the first-order rate constant for nonproductive substrate dissociation from P450-I (k_{-1}), and the first-order rate constant for substrate oxidation by P450-I (k_2). k_{obs} is the observed rate of substrate oxidation. The relationship between k_{obs} and the other rate constants is given in the SOM text.

P450 chemistry. Perferryl [iron(V)oxo] and ferric hydroperoxo complexes have been suggested as alternative hydroxylating agents (*2*, *4*, *34*–*36*). The perferryl species has been proposed to be the immediate product of oxygen activation, but evidence for its existence is lacking. The hydroperoxo complex has been prepared and characterized. However, experiments have ruled out its involvement in the hydroxylation step (*14*).

Our understanding of C-H bond activation in P450s has stagnated for want of a system in which P450-I could be prepared in high yield. Here, we report a breakthrough on this front (Fig. 1). We have found that highly purified preparations of CYP119, the thermophillic P450 from *Sulfolobus acidocaldarius* (*37*–*39*), allow the generation of compound I in unprecedented yields. In what follows, we detail the spectroscopic and kinetic characterization of CYP119-I.

Spectroscopic characterization of P450 compound I. When a 20 μM ferric enzyme solution (buffered to pH 7) was mixed (1:1) with a 40 μM *m*-chloroperbenzoic acid (*m*-CPBA) solution, we observed approximately 70% conversion to P450-I 35 ms after mixing (Fig. 2) (*40*). Multiple isosbestic points in the stopped-flow data set from 0 to 35 ms indicate the presence of only two UV/visible absorbing species: ferric enzyme and compound I. The dashed line in Fig. 2 gives the spectrum of CYP119-I. Because the 0-to-35-ms data set comprises only two absorbing species, the CYP119-I spectrum can be obtained with difference techniques or through the use of target testing (*41*). The spectrum of CYP119-I shown in Fig. 2 is in good agreement with the UV/visible spectrum reported previously by Kellner *et al.* (*21*).

Although a number of researchers have been able to observe P450-I in stopped-flow reactions (*20*–*22*), none have been able to prepare the intermediate using rapid freeze-quench techniques. This has been a rather puzzling aspect of P450 chemistry. The intermediate has been observed on time scales that are amenable to freeze-quenching. Yet all attempts to prepare P450-I with this technique have failed. The reason such efforts have gone unrewarded is not clear, but many have concluded that the intermediate is simply too reactive to be trapped. To determine whether unwanted side reactions (at the millimolar concentrations used in freeze-quench reactions) could be a detriment to compound I formation, high-concentration stopped-flow experiments were performed (fig. S2). These experiments, which revealed no substantial change in the compound I decay rate, suggested that CYP119-I could be prepared at millimolar concentrations by use of freeze-quench techniques.

With hopes of preparing CYP119-I samples for further spectroscopic characterizations, we performed freeze-quench experiments. Ferric CYP119 (3 mM) was mixed (2:1) with a 12 mM solution of *m*-CPBA, and the aqueous reaction mixture was sprayed into liquid ethane (89 K) 3.5 ms after mixing. Liquid ethane was subsequently removed under vacuum in an isopentane bath (~120 K), after which the samples were packed under liquid nitrogen.

Mössbauer measurements on the freeze-quenched samples confirmed the formation of P450-I in ~75% yield. The spectra shown in Fig. 3 were obtained by subtracting the spectrum of ferric CYP119 (25%) from the raw data [fig. S3 and supporting online material (SOM) text]. Spectrum A/B was obtained with a 54-mT field applied parallel/perpendicular to the γ-beam. These spectra were fit simultaneously (solid lines) assuming an effective $S = 1/2$ representation (SOM text). The parameters obtained from these fits are listed (along with the values obtained for CPO-I) in Table 1. The Mössbauer parameters and spectra of the CYP119 intermediate are similar to those reported for CPO-I (*23*). This similarity facilitates assignment of the CYP119 intermediate: It is best described as having an iron(IV)oxo unit exchange coupled to a ligand-based radical—the elusive P450 compound I.

Although CPO-I and CYP119-I have similar UV/visible and Mössbauer spectra, their electron paramagnetic resonance (EPR) signatures are different (Fig. 4). EPR measurements of freeze-quenched samples reveal the presence of CYP119-I, ferric CYP119, and at least two additional paramagnetic species. The spectra of these additional species (presumably protein-based radicals, although *m*-chlorobenzoic acid radicals have not been ruled out) overlap the CYP119-I spectrum but are easily differentiated by their temperature and power dependence (fig. S4). Like CPO-I, CYP119-I is fast-relaxing, and EPR signals associated with the intermediate can be observed only below ~25 K (*23*). As a result, the spectrum of CYP119-I can be extracted from measurements at low temperature and high power. Under the appropriate conditions, the signals of the other paramagnetic species can be fully saturated, and the spectrum of CYP119-I can be obtained by difference. The spectrum of CYP119-I shown in Fig. 4 was obtained by taking the difference of spectra obtained at 7.5 K using 203-mW and 128-mW microwave power (fig. S4).

The electronic structure of P450 compound I is best described as an $S = 1$ iron(IV)oxo unit exchange coupled with an $S = 1/2$ ligand-based radical. This exchange coupling (J) produces doublet and quartet states, which are mixed by the strong zero-field splitting (D) of the ferryl moiety. These interactions split the system into three-Kramers doublets, only the lowest of which is populated and EPR-active. As a result, the system may be modeled in an effective $S = 1/2$ representation (*23*). The g values of this effective representation can be shown to be functions of the ferryl g values and the ratio of J/D (SOM text and eq. S3). Fits of the CYP119-I data yield $g^{eff} = (1.86, 1.96, 2.00)$. These values are indicative of antiferromagnetic coupling and $|J|/D = 1.3$ (*42*). Similar procedures for CPO-I yield $g^{eff} = (1.61, 1.72, 2.00)$ and $|J|/D = 1.02$—values in good agreement with those reported by Rutter *et al.* (*23*). The increased $|J|/D$ in CYP119-I pushes $g_{\perp}^{eff}$ to lower fields, altering the shape of the spectrum relative to CPO-I. This effect is illustrated with simulated absorption spectra in Fig. 4C. The factors resulting in the increased $|J|/D$ in CYP119-I are not known. We have reported that axial-ligand

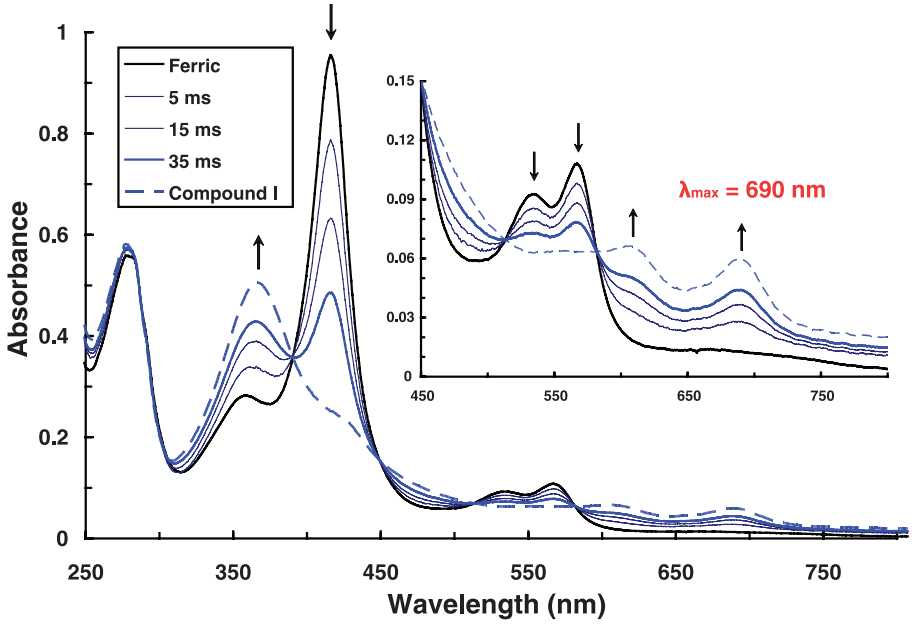

Fig. 2. UV/visible spectra obtained from the stopped-flow mixing (1:1) of 20 μM ferric CYP119 with 40 μM *m*-CPBA at 4°C. The blue traces correspond to spectra taken 5, 15, and 35 ms after mixing. Maximum yield of P450-I was ~70% at 35 ms. At later times, isosbestic points were lost, and a portion of the protein was degraded from the use of excess *m*-CPBA as judged by the final Reinheitszahl ($R_z = Abs_{416\ nm}/Abs_{280\ nm}$) ($R_z$) of 1.31 (fig. S1). All spectral changes were completed within 2.5 s. Dashed line indicates the spectrum of CYP119 compound I obtained by difference techniques (*41*).

spin density favors antiferromagnetic coupling (*43*). A larger value of $|J|$ could be the hallmark of increased sulfur spin density or a shortened Fe-S bond. It is unclear how these factors would affect the zero-field splitting.

Kinetic characterization of P450 compound I. The natural substrate of CYP119 is unknown, but previous work has shown that CYP119 oxidizes long-chain fatty acids (*44*). CYP119 binds these C_{10}- to C_{20}-sized saturated hydrocarbons with micromolar affinity and hydroxylates them at the ω- through ω-3 positions (*44*, *45*). The reaction with lauric acid (C_{12}) is the best characterized, kinetically. Under turnover conditions, CYP119 hydroxylates lauric acid at a rate of $k_{cat} = 11\ min^{-1}$ (*45*). One expects direct oxidation by compound I to be many orders of magnitude faster.

To investigate the rate at which compound I hydroxylates unactivated hydrocarbons, reactions of CYP119-I with hexanoic, octanoic, and dodecanoic acids (C_6, C_8, C_{12}), their perdeuterated forms, and camphor (the natural substrate of $P450_{cam}$) were studied at 4°C under pseudo first-order conditions by using stopped-flow techniques. In a typical kinetic experiment, CYP119 was premixed with one equivalent of *m*-CPBA and aged until exponential decay of compound I was apparent (100 ms). This solution, typically consisting of 35 to 40% compound I, was then mixed with a solution containing the desired substrate. This process allowed for the reaction of ~2.5 μM CYP119-I with varying substrate concentrations. Progress of the reaction was monitored by following the return of ferric enzyme (416 nm) or the decay of compound I (690 nm). Kinetic traces showed good single-exponential behavior for more than six half-lives (figs. S8 to S11). Fits of these traces provided observed rate constants, k_{obs}. Plots of k_{obs} versus substrate concentration were linear and provided apparent second-order rate constants, k_{app}, for the oxidation of substrate by CYP119-I (Fig. 5, Table 2, and SOM text). The ability of CYP119 to hydroxylate substrates using *m*-CPBA was verified with gas chromatography–mass spectrometry (GC-MS) (fig. S5).

The apparent second-order rate constants for substrate oxidation by CYP119-I are listed in Table 2. The rate constant for the oxidation of lauric acid is a remarkably efficient $k_{app} = 1.1 \times 10^7\ M^{-1}s^{-1}$. In the presence of 20 μM lauric acid, the observed rate of compound I decay is $220\ s^{-1}$.

The kinetic parameters listed in Table 2 reveal an interesting trend in fatty acid oxidation. The apparent second-order rate constant for substrate oxidation is a function of chain length. On going from C_6 to C_{12}, k_{app} increases by ~10^3. Plots of ln (k_{app}) versus chain length suggest a linear free-energy relationship—possibly derived from the free energy of binding. The perdeuterated substrates show an even larger (~10^4) increase in rate constant. As a result, the isotope effects obtained from these rate constants ($KIE_{obs} = {}^{H}k_{app}/{}^{D}k_{app}$) also show variation, but the trend is reversed: The observed kinetic isotope effects (KIEs) decrease with chain length. The variation in KIE can be understood in terms of the mechanism shown in Fig. 1.

Under nonsaturating conditions, the KIEs for strongly bound substrates are masked. The full unmasked values can be obtained only when nonproductive substrate dissociation is rapid as compared with substrate oxidation (SOM text). The observed KIEs are determined by the relative magnitudes of k_{-1} and k_2. For highly reactive intermediates and strong substrate binding (${}^{H}k_2$, ${}^{D}k_2 >> k_{-1}$), substrate association is rate limiting, $k_{obs} = [S]k_1$. Under these conditions, $k_{app} = k_1$ and an isotope effect of $KIE_{obs} = 1.0$ is predicted (for example, lauric acid). With decreasing substrate affinity ($C_6 < C_8 << C_{12}$), k_{-1} increases relative to k_2, and KIE_{obs} grows from the limiting value of 1.0 toward the full unmasked value of ${}^{H}k_2/{}^{D}k_2$. This latter value is obtained only when substrate binding is in rapid equilibrium ($k_{-1} >> {}^{H}k_2$, ${}^{D}k_2$). Under these conditions, $k_{app} = K_e k_2$, where $K_e = k_1/k_{-1}$ is the equilibrium constant.

The preceding analysis provides the second-order rate constant for lauric acid association, $k_1 = k_{app} = 1.1 \times 10^7\ M^{-1}s^{-1}$. Assuming a dissociation constant (K_d) similar to that of ferric enzyme ($K_d = 1\ \mu M$), one obtains a value of $k_{-1} \sim 10\ s^{-1}$ for the rate of nonproductive lauric acid dissociation, whereas the largest measured value of k_{obs} provides a lower limit for the rate of lauric acid oxidation, $k_2 > 210\ s^{-1}$. These values are consistent with the conditions required (${}^{H}k_2$, ${}^{D}k_2 >> k_{-1}$) for an observed isotope effect of $KIE_{obs} = 1.0$.

P450 hydroxylations are subject to large intrinsic isotope effects, and the observation of unmasked KIEs ≥ 10 is typical (*3*, *4*). These KIEs, which indicate substantial hydrogen tunneling, are larger than the value obtained from semiclassical arguments, $KIE_{SC} \sim 7$ (*46*). As a result, we may use KIE_{SC} to provide a lower limit for the rate of bound lauric acid oxidation (${}^{H}k_2$). Assuming KIE ≥ 7, one obtains ${}^{H}k_2 \geq 1400\ s^{-1}$.

This report confirms not only the existence but the catalytic competence of P450-I. CYP119-I

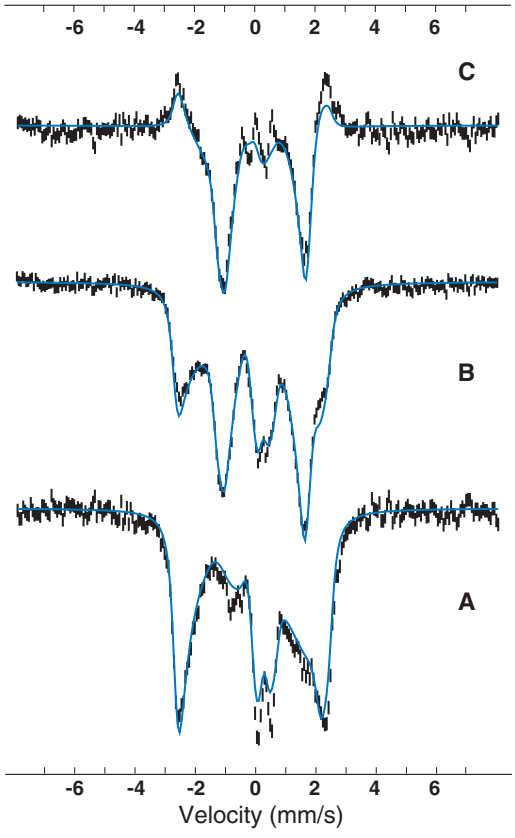

Fig. 3. Mössbauer spectra of CYP119 compound I at a temperature of 4.2 K, obtained by subtracting the spectrum of ferric CYP119 (25%) from the raw data (fig. S3 and SOM text). A 54-mT field was applied parallel to the γ-beam for spectrum A and perpendicular to the γ-beam for B. Spectrum C is the A-B difference spectrum. Solid lines are best fits of the data. Spectra A and B were fit simultaneously, assuming an effective $S = 1/2$ representation (SOM text, fitting details). Fit parameters are listed in Table 1. CYP119-I samples were prepared by mixing (2:1) ferric CYP119 (3 mM, $R_z \geq 1.65$, in 100 mM Kphos buffer, pH 7.0) with a solution of *m*-CPBA (12 mM, in 20:80 acetonitrile:water).

Table 1. Mössbauer and EPR parameters for P450-I and CPO-I. The relationship between the effective *g* values, *J*/*D*, and the ferryl *g* values can be found in (*40*). See (*42*) for a discussion of the ferryl *g* values. The intrinsic ferryl hyperfine couplings were obtained by fitting the Mössbauer data in the coupled representation.

	δ (mm/s)	ΔE_Q (mm/s)	Effective $S = 1/2$ representation							Ferryl values						
			g_x	g_y	g_z	A_x (T)	A_y (T)	A_z (T)	*J*/*D*	g_x	g_y	g_z	A_x (T)	A_y (T)	A_z (T)
CPO-I	0.13	0.96	1.72	1.61	2.00	−31	−30	−2	1.02	2.27	2.19	2.00	−24	−22	−2
CYP119-I	0.11	0.90	1.96	1.86	2.00	−28	−32	−3	1.30	2.27	2.20	2.00	−20	−23	−3

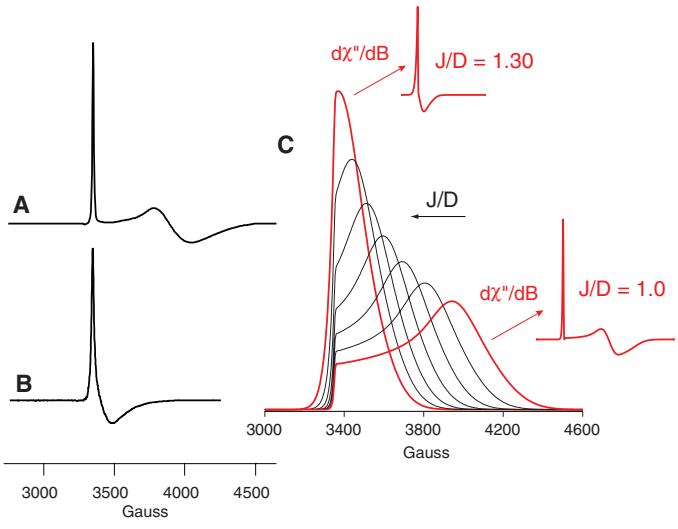

Fig. 4. (**A**) EPR spectrum of CPO-I at a temperature of 8 K taken with 203-mW microwave power. (**B**) EPR spectrum of CYP119-I at a temperature of 7.5 K. The CYP119-I spectrum was obtained from the difference of spectra taken with 203-mW and 128-mW microwave power (fig. S4). At these high powers, signals associated with other paramagnetic species are fully saturated, whereas the CYP119-I signal continues to grow with increasing power. Fits of the CPO-I and CYP119-I EPR spectra can be found in (*40*). (**C**) Effect of *J*/*D* on the EPR spectrum is best illustrated through a comparison of simulated absorption spectra. The simulations were performed with the ferryl *g* values listed in Table 1. *J*/*D* changes from 1.0 to 1.3 across the series (0.05 increments). The derivative of the *J*/*D* = 1.0 simulation resembles the CPO-I spectrum shown in (A). The derivative of the *J*/*D* = 1.30 spectrum resembles the CYP119-I spectrum shown in (B).

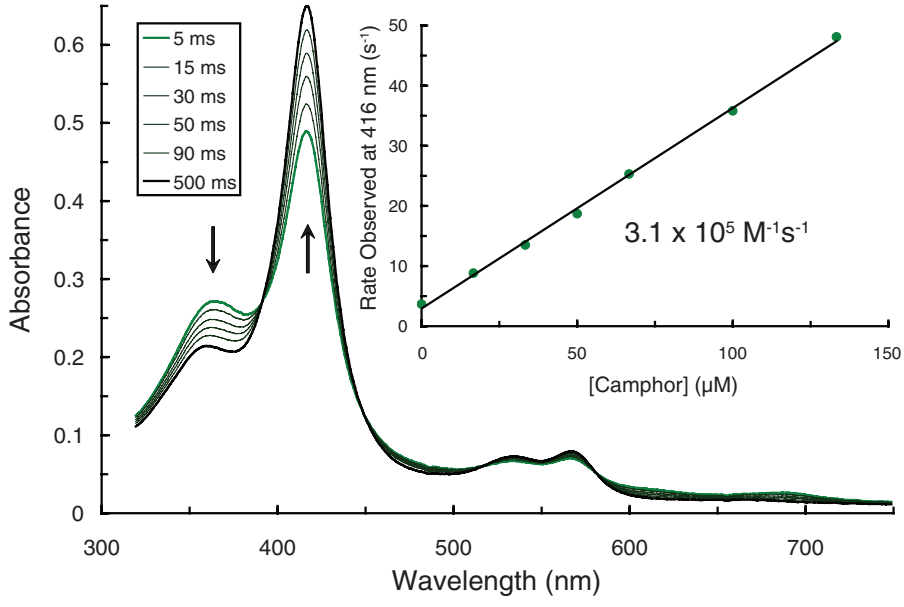

Fig. 5. UV/visible spectra taken during the reaction of CYP119-I with 50 μM camphor at 4°C. In a typical kinetic experiment, 20 μM CYP119 (100 mM Kphos pH 7.0) was premixed with one equivalent of *m*-CPBA and aged until exponential decay of compound I was apparent (100 ms). This solution, which typically consisted of 35 to 40% compound-I, was then mixed with a solution containing the desired substrate (100 mM Kphos pH 7.0). This process allowed for the reaction of ~2.5 μM CYP119-I, with varying concentrations of substrate. The UV/visible traces were taken at the times listed after the final mix. Singular value decomposition analysis indicated that only two UV/visible absorbing species were present in the reaction. (Inset) Observed CYP119-I decay rate versus camphor concentration.

Table 2. Apparent second-order rate constants at 4°C, observed isotope effect, and substrate concentration range for CYP119-I oxidations.

Substrate	$^{H}k_{app}$ (M^{-1} s^{-1})	$^{D}k_{app}$ (M^{-1} s^{-1})	KIE_{obs}	[^{H}S]/[^{D}S]
Camphor	3.5 (±0.1) × 10^5	—	—	0 to 266 μM/–
Hexanoic acid	4.4 (±0.6) × 10^4	3.5 (±0.8) × 10^3	12.5	0 to 5 mM/0 to 12 mM
Octanoic acid	4.5 (±0.3) × 10^5	8.6 (±0.5) × 10^4	5.3	0 to 533 μM/0 to 1.3 mM
Dodecanoic (lauric) acid	1.1 (±0.1) × 10^7	1.1 (±0.3) × 10^7	1.0	0 to 17 μM/0 to 17 μM

is capable of oxidizing unactivated hydrocarbons with an apparent second-order rate constant of $k_{app} = 1.1 \times 10^7$ $M^{-1}s^{-1}$. The large intrinsic KIE (≥12.5) observed in the direct oxidation of substrate is consistent with values obtained from intramolecular competition studies (*3*, *4*). Its magnitude supports a mechanism in which compound I abstracts hydrogen from substrate, forming an iron(IV)hydroxide that rapidly recombines with substrate to yield hydroxylated product: the rebound mechanism as postulated by Groves.

References and Notes

1. P. R. O. de Montellano, Ed., *Cytochrome P450: Structure, Mechanism, and Biochemistry* (Kluwer Academic/Plenum, New York, ed. 3, 2005).
2. I. G. Denisov, T. M. Makris, S. G. Sligar, I. Schlichting, *Chem. Rev.* **105**, 2253 (2005).
3. J. T. Groves, G. A. McClusky, R. E. White, M. J. Coon, *Biochem. Biophys. Res. Commun.* **81**, 154 (1978).
4. P. R. Ortiz de Montellano, *Chem. Rev.* **110**, 932 (2010).
5. T. M. Makris, K. von Koenig, I. Schlichting, S. G. Sligar, *J. Inorg. Biochem.* **100**, 507 (2006).
6. H. M. L. Davies, J. R. Manning, *Nature* **451**, 417 (2008).
7. K. Godula, D. Sames, *Science* **312**, 67 (2006).
8. B. M. Hoffman, *Proc. Natl. Acad. Sci. U.S.A.* **100**, 3575 (2003).
9. J. T. Groves, *Proc. Natl. Acad. Sci. U.S.A.* **100**, 3569 (2003).
10. L. Que Jr., Y. Watanabe, *Science* **292**, 651 (2001).
11. K. D. Karlin, *Nature* **463**, 168 (2010).
12. S. G. Sligar, T. M. Makris, I. G. Denisov, *Biochem. Biophys. Res. Commun.* **338**, 346 (2005).
13. I. Schlichting *et al.*, *Science* **287**, 1615 (2000).
14. R. Davydov *et al.*, *J. Am. Chem. Soc.* **123**, 1403 (2001).
15. V. Schünemann, C. Jung, J. Terner, A. X. Trautwein, R. Weiss, *J. Inorg. Biochem.* **91**, 586 (2002).
16. I. G. Denisov *et al.*, *J. Inorg. Biochem.* **87**, 215 (2001).
17. I. G. Denisov, T. M. Makris, S. G. Sligar, *J. Biol. Chem.* **276**, 11648 (2001).
18. R. Davydov *et al.*, *J. Am. Chem. Soc.* **127**, 1403 (2005).
19. S. H. Kim *et al.*, *Dalton Trans.* **21**, 3464 (2005).
20. T. Egawa, H. Shimada, Y. Ishimura, *Biochem. Biophys. Res. Commun.* **201**, 1464 (1994).
21. D. G. Kellner, S. C. Hung, K. E. Weiss, S. G. Sligar, *J. Biol. Chem.* **277**, 9641 (2002).
22. T. Spolitak, J. H. Dawson, D. P. Ballou, *J. Biol. Chem.* **280**, 20300 (2005).
23. R. Rutter *et al.*, *Biochemistry* **23**, 6809 (1984).
24. M. T. Green, J. H. Dawson, H. B. Gray, *Science* **304**, 1653 (2004).
25. K. L. Stone, R. K. Behan, M. T. Green, *Proc. Natl. Acad. Sci. U.S.A.* **102**, 16563 (2005).
26. T. Egawa *et al.*, *FEBS Lett.* **305**, 206 (1992).
27. S. H. Kim, R. Perera, L. P. Hager, J. H. Dawson, B. M. Hoffman, *J. Am. Chem. Soc.* **128**, 5598 (2006).
28. K. L. Stone, R. K. Behan, M. T. Green, *Proc. Natl. Acad. Sci. U.S.A.* **103**, 12307 (2006).
29. F. van Rantwijk, R. A. Sheldon, *Curr. Opin. Biotechnol.* **11**, 554 (2000).
30. A. Zaks, D. R. Dodds, *J. Am. Chem. Soc.* **117**, 10419 (1995).
31. R. Zhang, N. Nagraj, D. S. Lansakara-P, L. P. Hager, M. Newcomb, *Org. Lett.* **8**, 2731 (2006).
32. Recent reports have advocated the use of peroxynitrite and laser flash photolysis (LFP) to generate a species that has been assigned as CYP119-I (*34*). However, critical flaws in the preparation of this species have been noted (*33*). The UV/visible spectrum of the LFP-generated species bears no resemblance to the UV/visible spectrum of CYP119-I described in this or other work (*21*). The spectrum of the LFP-generated species resembles that of ferric enzyme. The LFP-generated species is reported to oxidize lauric acid at a rate of 0.8 s^{-1}. This is at least 2000 times slower than CYP119-I. No spectroscopic characterizations of the LFP-generated species other than UV/visible have been reported. We have recently suggested that the LFP-generated intermediate is not compound I (*41*).
33. R. K. Behan, L. M. Hoffart, K. L. Stone, C. Krebs, M. T. Green, *J. Am. Chem. Soc.* **129**, 5855 (2007).

34. Q. Wang, X. Sheng, J. H. Horner, M. Newcomb, *J. Am. Chem. Soc.* **131**, 10629 (2009).
35. R. E. P. Chandrasena, K. P. Vatsis, M. J. Coon, P. F. Hollenberg, M. Newcomb, *J. Am. Chem. Soc.* **126**, 115 (2004).
36. M. Newcomb *et al.*, *J. Am. Chem. Soc.* **125**, 6064 (2003).
37. R. L. Wright, K. Harris, B. Solow, R. H. White, P. J. Kennelly, *FEBS Lett.* **384**, 235 (1996).
38. M. A. McLean, S. A. Maves, K. E. Weiss, S. Krepich, S. G. Sligar, *Biochem. Biophys. Res. Commun.* **252**, 166 (1998).
39. K. S. Rabe, K. Kiko, C. M. Niemeyer, *ChemBioChem* **9**, 420 (2008).
40. Materials and methods are available as supporting material on *Science* Online.
41. J. Rittle, J. M. Younker, M. T. Green, *Inorg. Chem.* **48**, 3610 (2010).
42. Although it is clear from our fitting—as well as the spectra displayed in Fig. 4—that $|J|/D$ in CYP119-I has increased substantially relative to its value in CPO-I, the magnitude of the increase is not definite. The actual value of J/D depends critically on the choice of ferryl g values, for which only estimates are available. In our analysis, we have obtained ferryl g values by fitting CPO-I under the assumption that $|J|/D = 1.02$, as originally reported by Rutter *et al.* (*23*). This procedure provided the ferryl g values listed for CPO-I in Table 1, which were then used as input for the fitting of CYP119-I. The ferryl g values obtained for both species are reasonably similar to the CPO-I values ($g\perp = 2.28$ and $g\| = 1.94$) used by Rutter *et al.*, who modeled but did not fit their CPO-I data. Our ferryl g values result in a 27% increase in $|J|/D$ relative to CPO, whereas the values of Rutter *et al.* result in an increase of 24%. Recently, it was suggested that $g\perp = 2.0$ may be more appropriate for the ferryl moiety (*27*). If this report is accurate, it would suggest that the ratio of $|J|/D$ in CYP119-I is almost twice as large as the value observed for CPO-I.
43. M. T. Green, *J. Am. Chem. Soc.* **123**, 9218 (2001).
44. L. S. Koo, C. E. Immoos, M. S. Cohen, P. J. Farmer, P. R. Ortiz de Montellano, *J. Am. Chem. Soc.* **124**, 5684 (2002).
45. Y. R. Lim *et al.*, *J. Microbiol. Biotechnol.* **20**, 574 (2010).
46. J. P. Klinman, in *Quantum Tunnelling in Enzyme-Catalysed Reactions*, R. K. Allemann, N. S. Scrutton, Eds. (The Royal Society of Chemistry, Cambridge, 2009), pp. 132–157.
47. This work was supported by NSF. We thank T. Grove and J. C. Calixto Moreno for assistance with GC-MS and C. Krest for help with preliminary EPR experiments. The CYP119 plasmid was graciously provided by P. R. Ortiz de Montellano.

Supporting Online Material

www.sciencemag.org/cgi/content/full/330/6006/933/DC1
Materials and Methods
Figs. S1 to S12
Table S1
References

9 June 2010; accepted 16 September 2010
10.1126/science.1193478

How the CCA-Adding Enzyme Selects Adenine over Cytosine at Position 76 of tRNA

Baocheng Pan,[1] Yong Xiong,[1] Thomas A. Steitz[1,2,3]*

CCA-adding enzymes [ATP(CTP):tRNA nucleotidyltransferases] add CCA onto the 3′ end of transfer RNA (tRNA) precursors without using a nucleic acid template. Although the mechanism by which cytosine (C) is selected at position 75 of tRNA has been established, the mechanism by which adenine (A) is selected at position 76 remains elusive. Here, we report five cocrystal structures of the enzyme complexed with both a tRNA mimic and nucleoside triphosphates under catalytically active conditions. These structures suggest that adenosine 5′-monophosphate is incorporated onto the A76 position of the tRNA via a carboxylate-assisted, one–metal-ion mechanism with aspartate 110 functioning as a general base. The discrimination against incorporation of cytidine 5′-triphosphate (CTP) at position 76 arises from improper placement of the α phosphate of the incoming CTP, which results from the interaction of C with arginine 224 and prevents the nucleophilic attack by the 3′ hydroxyl group of cytidine75.

CCA-adding enzymes are nucleotidyltransferases that catalyze the posttranscriptional addition of CCA onto the 3′ terminus of immature tRNAs without using a nucleic acid template (*1*). They are essential in all three kingdoms of life and are divided into two classes based on their sequences. The enzymes from Archaea belong to class I, whereas those from eubacteria and eukaryotes belong to class II (*2*). These two classes of enzymes may have quite different catalytic mechanisms.

During the past several years, crystal structures of CCA-adding enzymes and their tRNA complexes from Archaea (*3*–*7*), bacteria (*8*, *9*), and humans (*10*) have been determined. These structures show that both families have only one site for binding either cytidine 5′-triphosphate (CTP) or adenosine 5′-triphosphate (ATP). Though the crystal structures shed light on how class I CCA-adding enzymes achieve their specificity for addition of the second C at position 75 without the use of a nucleic acid template (*11*), the question of how A, rather than C, is added at position 76 remains controversial. Based on the crystal structures of ternary complexes prepared by diffusing nucleotides into preexisting crystals of an RNA-protein binary complex, two different models have been suggested. One proposal from studies of class I enzymes is that the specificity is conferred by the size and shape of the nucleotide-binding pocket that is determined by the movement of the flexible head domain (*5*). In contrast, another set of crystal structures of class I enzymes led to the conclusion that the discrimination is dictated by a single, flexible amino acid side chain (Arg^{224}) of the enzyme for addition of A76 (*6*).

To understand the structural basis of a biological process, structures of the entire assembly captured at each step in the process are necessary (*12*). The greatest challenge is to control the catalytic reaction of the nucleotide incorporation so that crystals of the whole assembly can be obtained at each step. The initial assembly is the ternary complex of the polymerase, the RNA primer, and the nucleotide triphosphate (NTP) substrate. Capturing this complex requires stopping its catalytic activity with strategies such as mutation of key amino acid residues (*13*), nonhydrolyzable NTP

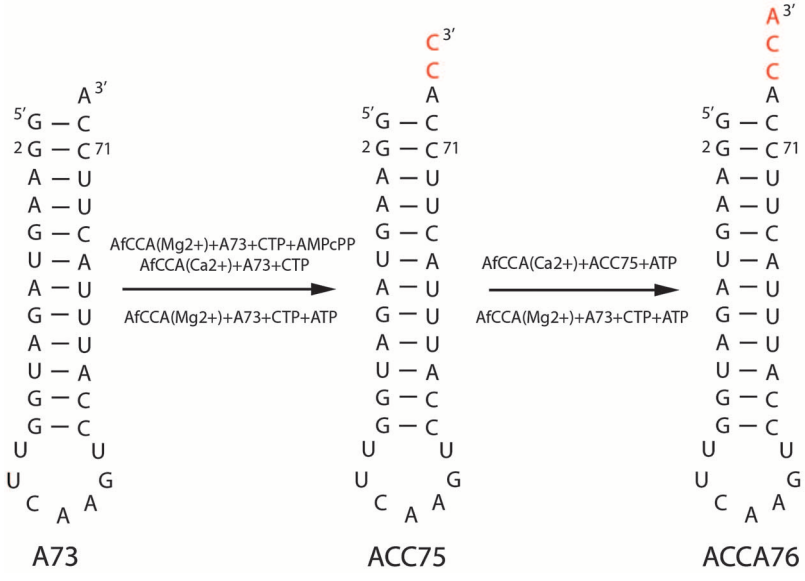

Fig. 1. Schematic diagram showing the tRNA mimics A73 and ACC75 that we used in the present study. The products of the reaction are shown on the right-hand side of the ternary complexes, with the nucleotides incorporated in the 3′ end of tRNA shown in red.

[1]Department of Molecular Biophysics and Biochemistry, Yale University, New Haven, CT 06520, USA. [2]Department of Chemistry, Yale University, New Haven, CT 06520, USA. [3]Howard Hughes Medical Institute, New Haven, CT 06520, USA.

*To whom correspondence should be addressed. E-mail: thomas.steitz@yale.edu